

Quantifying the Chirality of Vibrational Modes in Helical Molecular Chains

Ethan Abraham*

Department of Physics and Astronomy, University of Pennsylvania, Philadelphia, Pennsylvania 19104, USA

Abraham Nitzan

Department of Chemistry, University of Pennsylvania, Philadelphia, Pennsylvania 19104, USA and
School of Chemistry, Tel Aviv University, Tel Aviv 69978, Israel

(Dated: October 27, 2023)

The lack of quantitative methods for studying chirality has stunted our theoretical understanding of chirality-induced physical phenomena. The chiral phonon has been proposed to be involved in various physical phenomena, but it is not yet well defined mathematically. Here we examine two approaches for assigning and quantifying the chirality of molecular normal modes in double-helical molecular wires with various levels of twist. First, associating with each normal mode a structure obtained by imposing the corresponding motion on a common atomic origin, we apply the Continuous Chirality Measure (CCM) to quantitatively assess the relationship between the chirality-weighted normal mode spectrum and the chirality of the underlying molecular structure. We find that increasing the amount of twist in the double helix shifts the mean normal mode CCM to drastically higher values, implying that the chirality of molecular normal modes is strongly correlated with that of the underlying molecular structure. Second, we assign to each normal mode a pseudoscalar defined as the product of atomic linear and angular momentum summed over all atoms, and we analyze the handedness of the normal mode spectrum with respect to this quantity. We find that twisting the double-chain structure introduces asymmetry between right and left-handed normal modes so that in twisted structures different frequency bands are characterized by distinct handedness. This can give rise to global phenomena such as thermal chirality.

Among the concepts with such far-reaching consequences across science, perhaps none has remained as quantitatively elusive as *chirality*, defined as the breakage of all spatial mirror symmetry. While not impeding our understanding of its important consequences such as enantioselective catalysis and the homochirality of biological systems [1, 2], this elusiveness has restricted our ability to understand and predict the implications of chirality in many physical phenomena. As a recent example, there has been no consensus on the mechanism of *Chirality Induced Spin Selectivity* (CISS) [3, 4], a phenomenon wherein electron transmission through and accumulation in chiral materials exhibit strong spin selectivity.

The recently growing discussion of *chiral phonons* illustrates the importance and difficulty of rigorously addressing chirality in condensed matter. Over the past half decade, both local [5] and propagating [6] chiral phonons have been proposed to play important roles materials' electromagnetic phenomena, ranging from angular momentum transfer from photon to electron spin [7] and induction of magnetic fields [8] to spin selective transport [9–11] and calorimetric phenomena such as spin Seebeck effect [12].

Yet despite its prevalence in the literature, the chiral phonon is still ill-defined, often leading to ambiguities. The challenge is that motions in molecules and condensed matter must be compositions of excited normal vibrational modes, which are material specific and can possess non-trivial properties that undermine analogies with circularly polarized light (CPL) [13]. Phonon chirality is sometimes identified with angular momentum [5, 6]; however it is not obvious that angular mo-

mentum implies chirality. Unlike in static matter where chirality is better defined, with phonons the temporal dimension is now at play, and Ishito *et al.* [7] have pointed out that "true" chirality, where enantiomers are related by spatial inversion (\mathcal{P}), must be distinguished from "false" chirality, where enantiomers are related by time inversion (\mathcal{T}) followed by a spatial rotation (\mathcal{R}). Present descriptions of chiral phonons in crystal structures entail indirect inferences from the symmetry properties of a material's Brillouin zone [6, 7], but these approaches are not directly applicable to the analysis of chirality of molecular normal modes. Furthermore, The connection of the chirality of such modes and the chirality of the underlying molecular structure is not well understood although recent work indicates that such correlation does exist [14].

In the present work we introduce quantitative procedures to characterize the chirality of molecular vibrations. Furthermore we examine the correlation between the calculated normal mode chirality measure and the chirality of the underlying molecular equilibrium structure. This is a followup on our recent work [5], in which we used MD simulations to model a polyethylene double-helical wire with various levels of (left-handed) twist. Here, we use harmonic analysis of these structures to quantitatively explore the chirality of individual normal modes and their relationship to the chirality of the underlying molecular structure. The two-stranded polymer is an excellent model system for such a study because it can continuously vary between an achiral (untwisted) form and highly chiral (twisted) form. This allows us to use the chirality of the underlying structure as our independent variable. The results shown in this main text use polymers of length modeled by the TraPPE United Atom (UA) force field, which coarse grains each CH_x unit into a single interaction site [2, 3, 5]. The supplemental information (SI) confirms that our main find-

* abrahame@sas.upenn.edu

ings persist using other polymer lengths and force fields as well. We find that the normal mode spectra of twisted structures show strikingly more chiral features than the untwisted control.

Chirality Measure of Static Structures and Vibrational Modes. Chirality, to be distinguished from helicity, is defined as the breakage of mirror symmetry [18]. Such a property can be quantified using *continuous symmetry measures* [19], which assess the overlap of an object with the most similar object that contains the relevant symmetry. In the case of chirality, this means measuring the overlap of an object with its nearest achiral object. Naively, if $|Q\rangle$ is an object in a vector space V , then the nearest achiral object $|Q'\rangle = \frac{1}{2}(\mathbb{1} + \sigma)|Q\rangle$ is obtained by averaging $|Q\rangle$ with its enantiomer $\sigma|Q\rangle$, where σ is the reflection operator across the plane that maximizes the overlap $\langle Q|Q'\rangle$ (for an analytical method of finding this optimal mirror plane, see Ref. [19]). Since the quantity $\langle Q|Q'\rangle / \langle Q|Q\rangle$ is always unity for an achiral structure and at minimum 0 for a very chiral structure, it is a measure of the mirror symmetry content of $|Q\rangle$. This is the essence of the *Continuous Chirality Measure* (CCM), developed by Avnir *et al.* [19, 20], which (since chirality concerns the *absence* of mirror symmetry) is defined as

$$CCM(Q) = 1 - \frac{\langle Q|Q'\rangle}{\langle Q|Q\rangle}. \quad (1)$$

Note the CCM ranges from 0 to 1 with achiral objects having vanishing CCM and higher CCM implying higher chirality. In a standard application of this measure, the $|Q\rangle$ is a molecular structure represented by the root-mass-weighted atomic coordinates $|q_i\rangle = \sqrt{m_i}(x_i, y_i, z_i)^T$ defined relative to the center of mass, and its CCM can naturally be calculated according to

$$CCM(Q) = 1 - \frac{\sum_{i=1}^N \langle q_i | \mathbb{1} + \sigma | q_i \rangle}{2 \sum_{i=1}^N \langle q_i | q_i \rangle}. \quad (2)$$

Importantly, the same concept may be applied to define the chirality of any molecular normal mode $|u_k\rangle$ represented by atomic displacement vectors $|u_{k,i}\rangle = \sqrt{m_i}(u_{k,i}^x, u_{k,i}^y, u_{k,i}^z)^T$, evaluating the CCM by taking $|q_i\rangle \mapsto |u_{k,i}\rangle$ in Eq. (2). This makes it possible to assign a chirality measure to each normal mode, and in turn to evaluate the chirality-weighted molecular vibrational spectrum. Note that one weakness of the CCM measure, which we will address later in this text, is that it does not distinguish between enantiomers: opposite enantiomers have the same CCM value.

In Fig. 1 we show the results of such calculations, in which we have applied the CCM to our two-stranded wire's molecular structure and normal mode spectrum. Figure 1(a) shows the model system for this study, the two-stranded polyethylene wire with polymerization $N = 98$. Figure 1(b) shows the CCM of the molecular structure as a function of the number of twists; note that when we choose Q to be the entire wire (blue line), the CCM does not register twistedness. This is because the axial coordinates of the atoms $|q_i\rangle$ far from the center of mass dominate the inner products in Eq. (2), leading to low CCM values. When Q is taken to be the segment of the wire on a shorter length scale τ , the CCM is much more sensitive to the number of twists. We thus find that the CCM seems

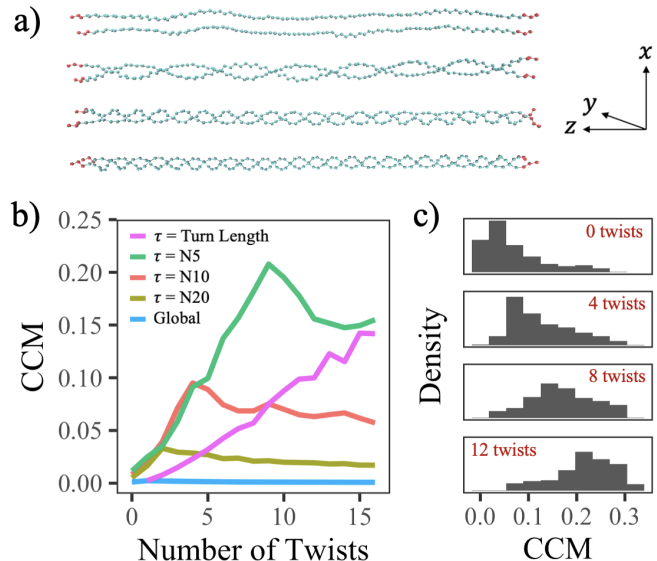


FIG. 1. (a) The model system for this study: a two-stranded $N = 98$ polyethylene wire containing various levels of twist (shown from top to bottom: 0, 4, 8, 12 twists). All twists are left-handed. The z -axis is taken to be the axis of the chains. Terminal atoms shown in red. (b) The CCM of the wire as a function of the number of twists. Results are shown when the structure Q is taken to be a segment of the wire corresponding to (pink) one helical turn, (green, red, gold) 5, 10, or 20 monomers, and (blue) the entire structure. (c) Histograms of the normal mode distribution binned by CCM for the structures shown in the top panel.

to be useful only when all three Cartesian dimensions of the structure examined are on the same order of magnitude. Note that when τ is chosen to be a unit turn of the helix (purple), the CCM is roughly proportional to the twistedness of the double-helix. In the other cases when τ is a fixed length, a maximum is obtained when the number of twists is $\sim 2\tau$.

Figure 1(c) shows the first key result of this work, which is that the distribution of normal modes, as measured by the CCM, is much more chiral when the underlying structure is more twisted. Note the CCM of the modes tend to be larger than the CCM of the structure. Contrary to the idea that chiral materials are necessary for chiral modes, we find that the majority of modes for the structure with 0 twists have a non-zero CCM; what changes with increased twist is the mean of the distribution. Note that since the vectors that represent the normal modes are displacements from equilibrium rather than locations in extended space, the length scale considerations for Fig. 1(b) are not relevant.

Momentum Pseudoscalar and Thermal Chirality. We have seen drastic trends in the phonon CCM distributions, yet the physical meaning of the CCM is unclear. The frequent association of chiral phonons with polarization in recent literature invites us to examine the angular momentum of the vibrational modes in our system. Various measures of vibration angular momentum have been proposed by Zhang and Niu, which refer either strictly to normal mode coordinates or also to the equilibrium position coordinates [21]. In this system it is natural to discuss the amplitude of the atomic angular momentum about the central axis. Figure 2(a) shows density polygons

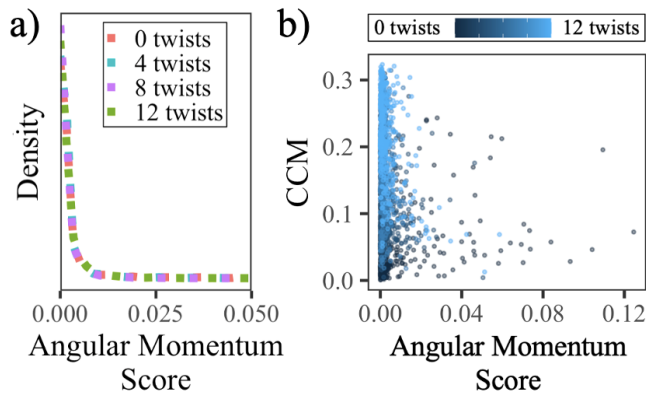


FIG. 2. (a) Frequency polygon showing the density of modes binned by angular momentum score (Eq. (3)) for the $N = 98$ polyethylene wire with selected amounts of twist. Lines are dashed so that they can be seen despite the fact that they all tend to coincide. (b) Scatter plots comparing CCM to the angular momentum score for individual normal modes. Lighter dots correspond to more twisted structures.

of the axial angular momentum in the normal modes of two-stranded polyethylene wires containing various levels of twist. The plotted *angular momentum score* (\tilde{L}_k^z) is calculated from the coefficients of each normal mode k

$$\tilde{L}_k^z = A_1 \left| \sum_i m_i (x_i u_{k,i}^y - y_i u_{k,i}^x) \right|, \quad (3)$$

where $u_{k,i}^\alpha$ is the displacement coefficient in Cartesian direction α for atom i atom in normal mode k , and where we have taken the coefficients have been normalized such that $\sum_i \sum_\alpha (u_{k,i}^\alpha)^2 = 1$. In this work, the tilde seen in Eq. (3) denotes a dimensionless score calculated from the normalized mode coefficients rather than a physical magnitude. The normalization coefficient A_1 in Eq. (3) is derived and justified in SI. There are two noteworthy observations. First is that we are forced to report the absolute value of the angular momentum score, for if a normal mode possesses axial angular momentum L_z at time t , clearly it will possess angular momentum $-L_z$ at time $t + \pi$. We thus note that angular momentum, on the level of individual vibrational modes, cannot define handedness. Secondly, we notice that the distribution of angular momentum possessed by the normal modes is insensitive to the chirality of the underlying structure: modes in the fully untwisted wire tend to carry just as much angular momentum as in the twisted structures. We conclude that angular momentum is not the defining feature of chiral modes. This conclusion is supported by Fig. 2(b) which shows that there is no obvious correlation between the angular momentum score and CCM for the modes of any structures examined.

Angular momentum proving insufficient as a chiral physical observable, we look to other fields for intuition regarding the physical meaning of chiral modes. In optics, Tang and Cohen recognized that chiral physical observable should be a time-even pseudoscalar [13]. This led them to define the chiral density of a field \mathbf{A} as

$$C = \mathbf{A} \cdot \nabla \times \mathbf{A}. \quad (4)$$

When applied to the electromagnetic field ($C = \frac{\epsilon_0}{2} \mathbf{E} \cdot \nabla \times \mathbf{E} + \frac{1}{2\mu_0} \mathbf{B} \cdot \nabla \times \mathbf{B}$), this variable has been found to determine the magnitude of *circular dichroism* [13, 22]. It has also been suggested that the chirality of a massless particle be defined as the *helicity*, $h = \mathbf{p} \cdot \boldsymbol{\sigma} / |\mathbf{p}|$ (\mathbf{p} momentum; $\boldsymbol{\sigma}$ spin), or in the case of fluids $h = \mathbf{v} \cdot \boldsymbol{\omega}$ (\mathbf{v} velocity; $\boldsymbol{\omega} = \nabla \times \mathbf{v}$ vorticity) [23]. Similarly, when three ordered vectors ($\mathbf{v}_1, \mathbf{v}_2, \mathbf{v}_3$) characterize an object, it has been suggested that chirality be defined by the scalar triple product $\mathbf{v}_1 \cdot (\mathbf{v}_2 \times \mathbf{v}_3)$ [23–26]. What do these measures have in common? They are all pseudoscalars, are composed of the inner product of a vector and a pseudovector, and appeal to our intuition regarding a helical structure defined by circulation about a central axis with a component parallel to that axis. This is in contrast with angular momentum, which is a pseudovector involving only circulation around a central axis with no parallel component.

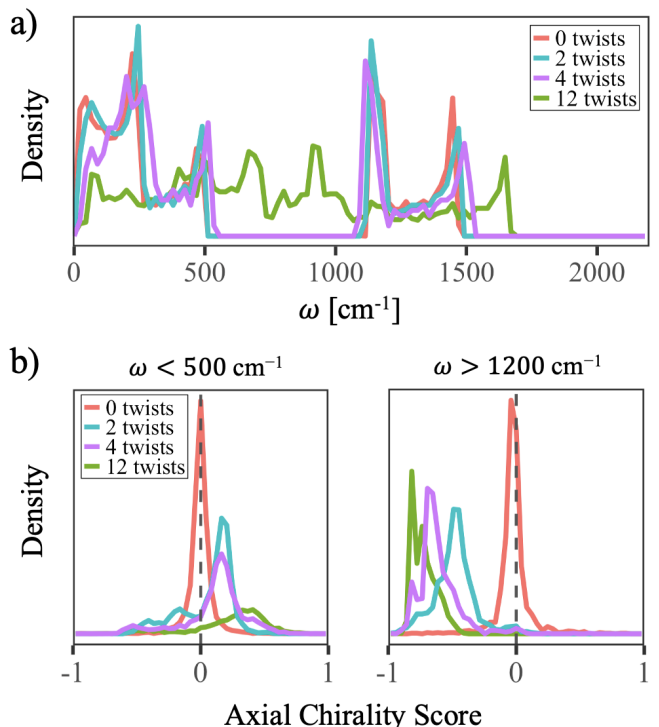


FIG. 3. (a) Frequency polygons showing the spectral densities of the two-stranded $N = 98$ polyethylene wire when the wire is (red) untwisted, or (blue, purple, green) containing 4, 8, and 12 twists. All twists are left-handed. (b) Frequency polygons showing the density of modes binned by axial chirality score (Eq. (5)) for the same structures as the top panel.

We now note that even if the CCM had understandable physical meaning, it is not a pseudoscalar and could not alone explain chiral interactions. In order to glean physical insight, we therefore suggest an analogy with Eq. (4) that $\mathbf{A} \mapsto \mathbf{p}$, and $\nabla \times \mathbf{A} \mapsto \mathbf{L}$. We refer to the resulting quantity $\mathbf{p} \cdot \mathbf{L}$ as the *momentum pseudoscalar*. The challenge is that unlike Eq. (4), evaluation of $\mathbf{p} \cdot \mathbf{L}$ depends on the choice of origin. Nevertheless, many chirality-dependent physical processes take place along a particular axis (e.g. an electron’s linear trajectory through a chiral material or a photon incident on a sample), so the essence of the behavior may be captured by the much

simpler pseudoscalar $p_z L_z$ where the z -axis is the axis of interest. In our present case where the z -axis is unique, we define the *axial chirality score* (\tilde{C}_k) of mode k as

$$\begin{aligned}\tilde{C}_k &= A_2 \sum_i \tilde{p}_{k,i}^z \tilde{L}_{k,i}^z \\ &= A_2 \sum_i m_i u_{k,i}^z (x_i u_{k,i}^y - y_i u_{k,i}^x).\end{aligned}\quad (5)$$

Like in Eq. (3), a normalization coefficient A_2 for this score is derived and justified in SI. The key intuition for the utility of Eq. (5) is that while the $\tilde{p}_{k,i}^z$ and $\tilde{L}_{k,i}^z$ each average to zero over the normal mode's temporal period, the product $\tilde{p}_{k,i}^z \tilde{L}_{k,i}^z$ is time symmetric, maintaining its sign throughout the period and thus having a nonzero average. Examining the density of modes with respect to this score instead of the CCM yields profound results. Figure 3 shows that like the CCM, twist tends to skew the distribution of \tilde{C}_k values away from zero, again indicating that chiral modes are associated with chiral structures. However, unlike the CCM, the this axial chirality score is signed and defines handedness. Remarkably, we see that different bands of the frequency spectrum (Fig. 3(a)) have different handedness when the structure is twisted. This result implies that that the thermal motion in a helical structure is inherently chiral.

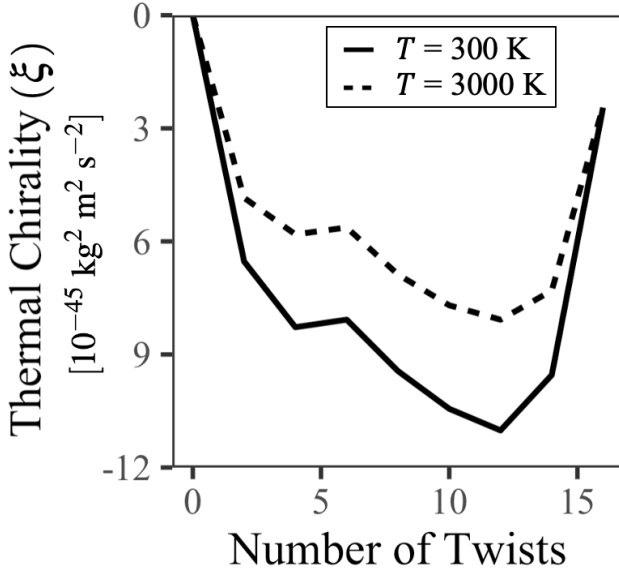


FIG. 4. Thermal chirality (Eq. (9)) plotted as a function of the number of twists for the two-stranded $N = 98$ polyethylene wire. The solid line denotes the results for $T = 300$ K while the dashed line denotes that for $T = 3000$ K. Note that the $T = 0$ line coincides with the $T = 300$ line to a good approximation (results not shown).

Now the quantity \tilde{C}_k is just a score to compare normal modes, but the frequency dependence of \tilde{C}_k suggests that the total axial chirality at thermal equilibrium might have interesting twist and temperature dependence. Specifically, the average quantity $\langle \tilde{p}_{k,i}^z \tilde{L}_{k,i}^z \rangle$ at thermal equilibrium can be calculated explicitly. The average kinetic energy possessed by mode k

with frequency ω_k is given by

$$\frac{1}{2} \langle E_k \rangle = \frac{\hbar \omega_k}{2} \left(\frac{1}{2} + \langle n(\omega_k) \rangle \right), \quad (6)$$

where $\langle n(\omega_k) \rangle$ is the mode's average occupancy. The average kinetic energy can also be written as

$$\frac{1}{2} \langle E_k \rangle = \sum_i \sum_\alpha \frac{1}{4} m_i (B_k u_{k,i}^\alpha)^2 \quad (7)$$

for some constant B_k that determines the amplitude of the mode's motion. Assuming that $m_i = m$ for all i and using $\sum_i \sum_\alpha (u_{k,i}^\alpha)^2 = 1$, substituting Eq. (6) and Eq. (7) implies that

$$B_k = \sqrt{\frac{2\hbar\omega_k}{m} \left(\frac{1}{2} + \langle n(\omega_k) \rangle \right)}. \quad (8)$$

Using the Bose-Einstein distribution $\langle n(\omega_k) \rangle = (e^{\hbar\omega_k/k_B T} - 1)^{-1}$, the total *thermal chirality* (ξ) is thus given by

$$\begin{aligned}\xi(T) &= \sum_k \sum_i \langle \tilde{p}_{k,i}^z \tilde{L}_{k,i}^z \rangle \\ &= \sum_k \sum_i (m B_k u_{k,i}^z) (m B_k (x_i u_{k,i}^y - y_i u_{k,i}^x)) \\ &= \sum_k \sum_i 2m\hbar\omega_k u_{k,i}^z (x_i u_{k,i}^y - y_i u_{k,i}^x) \left(\frac{1}{2} + \frac{1}{e^{\hbar\omega_k/k_B T} - 1} \right).\end{aligned}\quad (9)$$

The fact that the terms in Eq. 9 are nonzero follows intuitively from the fact that the momentum pseudoscalar is time-even.

In Fig. 4 we plot this thermal chirality measure as a function of the number of twists. We found that only at very large temperatures was a substantial deviation from the low temperature (solid line) obtained. The physical meaning of this quantity is yet to be fully explored, but we note that it is a global pseudoscalar determined only by the equilibrium thermal motion of the system that shows dependence on the chirality of the underlying structure.

The thermal chirality we have demonstrated hints at interesting phenomena such as chiral friction or chiral collisions. As a thought experiment, we may imagine a universe composed of a single (classical) free particle interacting with a single chiral harmonic mode k . We note that the ratio of the mode's angular and linear momentum is fixed throughout the entirety of its period ($L_k^z/p_k^z = \tilde{L}_k^z/\tilde{p}_k^z$). Combining this insight with conservation of both linear and angular momentum, we conclude that if the particle loses linear momentum δp_z to the mode, so too must it acquire angular momentum $\delta L_z = -(\tilde{L}_k^z/\tilde{p}_k^z)\delta p_z$. Granted in the reality of a many-body system, it would not be realistic to think of an isolated interaction of a particle with a single normal mode, and building a kinetic theory that makes use of the insight presented in this work remains a subject for future investigation. But this thought experiment, when combined with the asymmetry of the \tilde{C}_k over particular frequency ranges, could pave the way for explaining some chirality-induced physical phenomena.

Methods. A detailed description of how the twisted structures and normal modes were obtained can be found in Ref. [5]. The twisted structures were obtained from MD simulations in which a torque was applied to one end of the polymer wire while keeping the other end fixed using LAMMPS.

Normal modes and corresponding eigenfrequencies were calculated from energy minimized structures using GROMACS. Normal modes associated with imaginary frequencies were discarded from the analyses, but for all structures examined these composed $< 6\%$ of the spectrum. The CCM calculations were implemented using the `gsym` function of the `cosymb` library in Python. All CCM calculations assumed that the nearest achiral structure had S_1 symmetry, and the trivial permutation was forced in order to respect the information contained in bond connectivity. Calculations were repeated on multiple configurations sampled from the MD simulations and thermal fluctuations were found to be minor. The polymers were studied at their natural untwisted length by fixing ter-

minal atoms at either end. The force field used to model the polymers in the main text was the TraPPE-UA force field, but conclusions were cross-checked using other force fields; see SI.

Acknowledgements. The research of A.N. is supported by the Air Force Office of Scientific Research under award number FA9550-23-1-0368 and the University of Pennsylvania. E.A. acknowledges the support of the the University of Pennsylvania (Grant GfFMUR). The authors are grateful to Mohammadhasan Dinpajooh and Claudia Climent for technical assistance, and to David Avnir, Oded Hod, and Philip Nelson for useful discussions.

-
- [1] J. Gal, *Chirality* **20**, 5 (2008).
- [2] S. Honzawa, H. Okubo, S. Anzai, M. Yamaguchi, K. Tsumoto, and I. Kumagai, *Bioorganic and Medicinal Chemistry* **10**, 3213 (2002).
- [3] R. Naaman and D. H. Waldeck, *The Journal of Physical Chemistry Letters* **3**, 2178 (2012), pMID: 26295768.
- [4] F. Evers, A. Aharony, N. Bar-Gill, O. Entin-Wohlman, P. Hedegård, O. Hod, P. Jelinek, G. Kamieniarz, M. Lemesko, K. Michaeli, V. Mujica, R. Naaman, Y. Paltiel, S. Refaely-Abramson, O. Tal, J. Thijssen, M. Thoss, J. M. van Ruitenbeek, L. Venkataraman, D. H. Waldeck, B. Yan, and L. Kronik, *Advanced Materials* **34**, 2106629 (2022), <https://onlinelibrary.wiley.com/doi/pdf/10.1002/adma.202106629>.
- [5] H. Chen, W. Zhang, Q. Niu, and L. Zhang, *2D Materials* **6**, 012002 (2018).
- [6] H. Chen, W. Wu, J. Zhu, S. A. Yang, and L. Zhang, *Nano Letters* **21**, 3060 (2021), pMID: 33764075.
- [7] K. Ishito, H. Mao, Y. Kousaka, Y. Togawa, S. Iwasaki, T. Zhang, S. Murakami, J. ichiro Kishine, and T. Satoh, *Nature Physics* **19**, 35 (2022).
- [8] D. M. Juraschek, T. c. v. Neuman, and P. Narang, *Phys. Rev. Res.* **4**, 013129 (2022).
- [9] T. K. Das, F. Tassinari, R. Naaman, and J. Fransson, *The Journal of Physical Chemistry C* **126**, 3257 (2022), <https://doi.org/10.1021/acs.jpcc.1c10550>.
- [10] J. Fransson, *Phys. Rev. B* **102**, 235416 (2020).
- [11] M. Shiranzaei, S. Kalhöfer, and J. Fransson, *The Journal of Physical Chemistry Letters* **14**, 5119 (2023), pMID: 37249543.
- [12] K. Kim, E. Vetter, L. Yan, C. Yang, Z. Wang, R. Sun, Y. Yang, A. H. Comstock, X. Li, J. Zhou, L. Zhang, W. You, D. Sun, and J. Liu, *Nature Materials* **22**, 322–328 (2023).
- [13] Y. Tang and A. E. Cohen, *Phys. Rev. Lett.* **104**, 163901 (2010).
- [14] H. Chen, W. Wu, J. Zhu, Z. Yang, W. Gong, W. Gao, S. A. Yang, and L. Zhang, *Nano Letters* **22**, 1688 (2022), pMID: 35148114.
- [5] E. Abraham, M. Dinpajooh, C. Climent, and A. Nitzan, *J. Chem. Phys.* (2023), 10.1063/5.0171680.
- [2] B. Chen and J. I. Siepmann, *J. Phys. Chem. B* **103**, 5370 (1999).
- [3] S. J. Keasler, S. M. Charan, C. D. Wick, I. G. Economou, and J. I. Siepmann, *J. Phys. Chem. B* **116**, 11234 (2012).
- [18] P. W. Fowler (2005) pp. 321–334.
- [19] M. Pinsky, C. Dryzun, D. Casanova, P. Alemany, and D. Avnir, *J. Comput. Chem.* **29**, 2712 (2008).
- [20] C. Dryzun and D. Avnir, *ChemPhysChem* **12**, 197 (2011).
- [21] L. Zhang and Q. Niu, *Phys. Rev. Lett.* **112**, 085503 (2014).
- [22] M. L. Solomon, A. A. E. Saleh, L. V. Poulikakos, J. M. Abendroth, L. F. Tadesse, and J. A. Dionne, *Accounts of Chemical Research* **53**, 588 (2020), pMID: 31913015.
- [23] J. Ishioka, Y. H. Liu, K. Shimatake, T. Kurosawa, K. Ichimura, Y. Toda, M. Oda, and S. Tanda, *Phys. Rev. Lett.* **105**, 176401 (2010).
- [24] X. Wan, A. M. Turner, A. Vishwanath, and S. Y. Savrasov, *Phys. Rev. B* **83**, 205101 (2011).
- [25] N. P. Armitage, E. J. Mele, and A. Vishwanath, *Rev. Mod. Phys.* **90**, 015001 (2018).
- [26] G. P. Katsoulis, Z. Dube, P. B. Corkum, A. Staudte, and A. Emmanouilidou, *Phys. Rev. A* **106**, 043109 (2022).

Supplemental Information: Quantifying the Chirality of Vibrational Modes in Helical Molecular Chains

I. MOLECULAR MODELS

For the calculations in the main text, we have representing our polymers using the Transferable Potentials for Phase Equilibria (TraPPE) United Atom (UA) model, which treats each CH_x unit as a single particle [[S1–S3]]. This model is useful because it greatly reduces the computational cost, yet it has been shown to still perform with high accuracy for calculations of thermal conductance in hydrocarbons [[S4]]. It is based on a force field (FF) that represents bonds with harmonic potentials and includes also angle (3-body), dihedral (4-body potentials), and Lennard Jones potentials. The Hamiltonian is given by

$$H_{\text{molecule}} = \sum_i \frac{p_i^2}{2m_i} + \sum_i k_{bi}(l_i - l_{0i})^2 + \sum_i k_{\theta i}(\theta_i - \theta_{0i})^2 + \sum_i \sum_{n_i} \frac{C_{ni}}{2} [1 + (-1)^{n_i-1} \cos(n_i \phi_i)] + \sum_i \sum_j 4\epsilon_{ij} \left[\left(\frac{\sigma_{ij}}{r_{ij}} \right)^{12} - \left(\frac{\sigma_{ij}}{r_{ij}} \right)^6 \right], \quad (\text{S1})$$

where p_i and m_i are the momentum and mass of a given particle respectively, l_i, l_{0i} , θ_i, θ_{0i} , are the actual and equilibrium bond lengths and angles respectively, ϕ_i are the dihedral angles, and r_{ij} are the inter-particle separations. Accordingly, the parameters k_{bi} and $k_{\theta i}$ are the spring constants for the bonds and angles, and the C_{ni} are the constants that define the dihedral potentials. As in Ref. [S1], the above parameter values were chosen to fit observed physical properties.

As we have done in our previous work [[S5]], we have cross-checked our results with two other models: i) an Explicit Hydrogen (EH) model and ii) a simplified force field inspired by the Freely Joint Chain (FJC) model [[S6]]. The Explicit Hydrogen model uses the same Hamiltonian as above, except that the Hydrogen and Carbon atoms are treated as separate bodies and different parameter values are chosen as appropriate (see Appendix A in [[S5]]). The FJC force field is also a united atom model that conventionally omits the angular potentials, dihedral potentials, and Leonard Jones (LJ) potentials. In the present application, since our calculations pertain to wires with multiple strands, the omission of the Leonard Jones potentials would create a non-physical situation with no repulsive force between two chains. We, therefore, modify the FJC field to include the LJ potential and denote this force field as FJC*. Hence the Hamiltonian becomes

$$H_{\text{FJC}^*} = \sum_i \frac{p_i^2}{2m_i} + \sum_i k_{bi}(l_i - l_{0i})^2 + \sum_i \sum_j 4\epsilon_{ij} \left[\left(\frac{\sigma_{ij}}{r_{ij}} \right)^{12} - \left(\frac{\sigma_{ij}}{r_{ij}} \right)^6 \right], \quad (\text{S2})$$

using the same parameter values as the TraPPE-UA FF. It should be noted that this FJC* model allows the angles to relax from $\theta_0 = 114^\circ$ to 180° , changing the natural length of the polymer. In our previous work we reported FJC* results using multiple lengths [[S5]], but here for all FJC* results reported, we have adjusted the length to the new natural length of the polymer, which is equal to the contour length of the polymer when using the TraPPE-UA model.

II. CCM NORMAL MODE SPECTRA

In our main text we presented the key finding that increased twist skews the distribution of the CCM of normal modes away from zero to greater mean values. Here we show that this trend was remarkably consistent across various trials, chain lengths, and force field models. The top and middle panels of Fig. S1 show that the trend is consistent across trials. Here, different *trials*

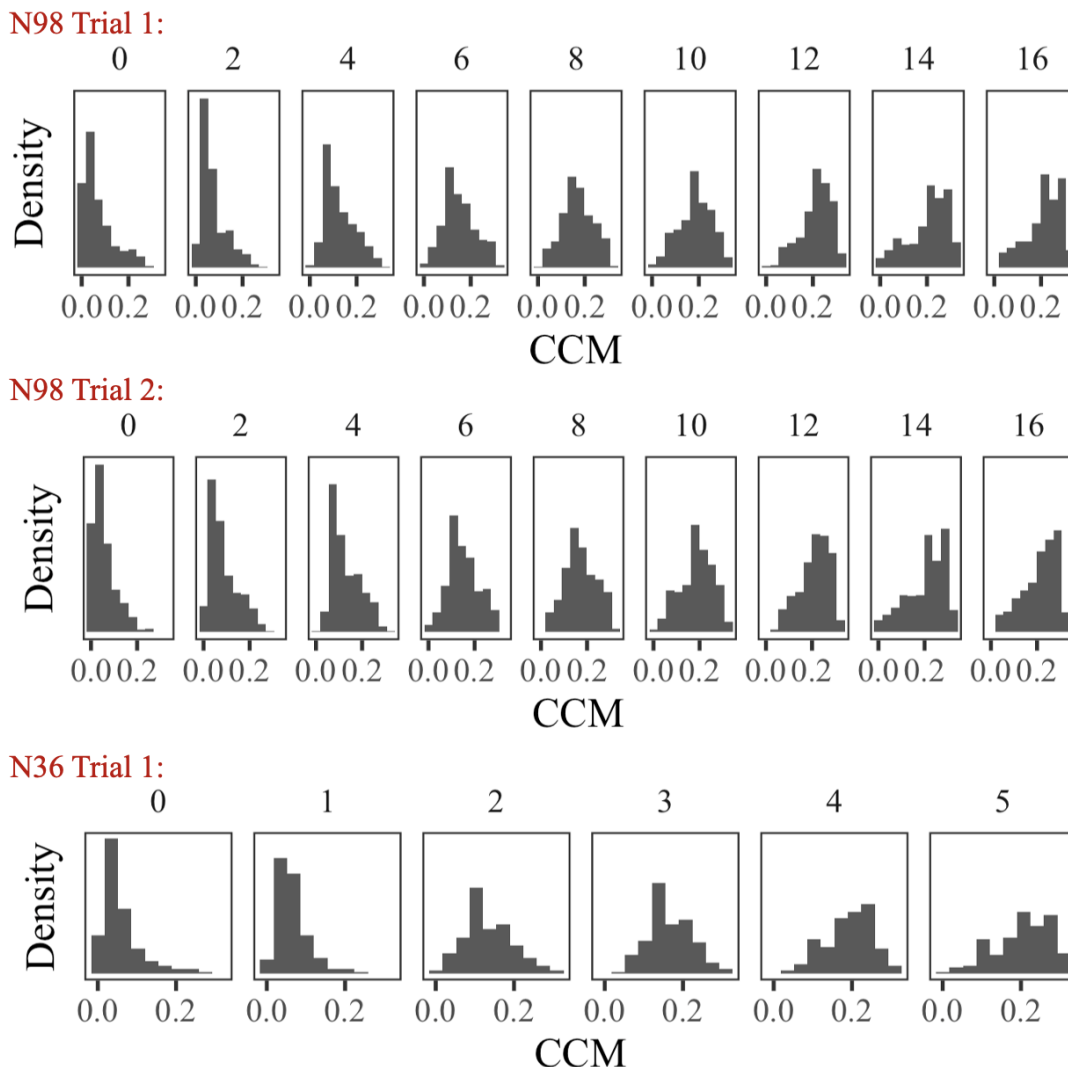


FIG. S1. (Top and middle) Histograms of the normal mode distribution binned by CCM for two stranded polyethylene wires of length $N = 98$ for various levels of twist. The number above each plot denotes the number of twists. Results are shown using two configurations of the same molecular structure sampled from two arbitrary timepoints throughout MD simulations. (Bottom) Same as above but for one trial of a polymers of length $N = 36$.

denote different configurations lifted from identically prepared molecular dynamics (MD) simulations. For a detailed description of such MD simulations, see our prior work [[S5]]. Although normal modes were computed from energy minimized structures, for molecules of this size there exist multiple local minima that have slightly different normal modes. We see that although the relative size of individual histogram bars varies slightly, there is no observable difference in the trend we have reported. Ten such trials have been checked (results not shown). The bottom panel shows that the same trend persists for a shorter chain length ($N = 36$).

Note that as one would expect, we cannot obtain as great an absolute number of twists N_T in the shorter chain as we could with a larger chain length. Such wires have been found to be characterized by a maximal number of twists $N_T^{\max}(N)$ before bonds begin to break. As shown in our previous work [[S5]], this is quantity $N_T^{\max}(N)$ is proportional (at least to a very good approximation) to the chain length of N . As such, when assessing the effect of twist on physical properties, the twist fraction $N_T/N_T^{\max}(N)$ is likely more fundamental than the absolute number of twists. Figure S2 shows that with respect to this parameter, the effect of twist on the mean of the distributions is consistent across chain lengths. Note that the CCM of these modes therefore

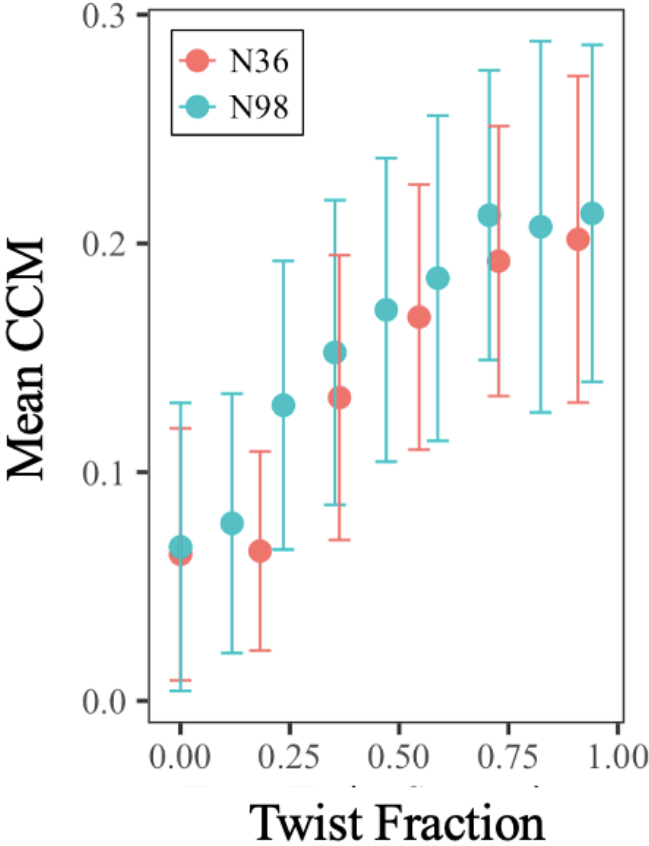


FIG. S2. The mean of the normal mode CCM distributions shown in trial 1 of Fig. S1 as a function of the Twist Fraction given by $N_T/N_T^{\max}(N)$. Results are shown for lengths (red) $N = 36$ and (blue) $N = 98$. Error bars show the standard deviation of the distributions.

appears to be independent of the absolute number of atoms in the structure. This was not the case when the CCM was applied to the *structure* as opposed to the modes, as discussed in the main text.

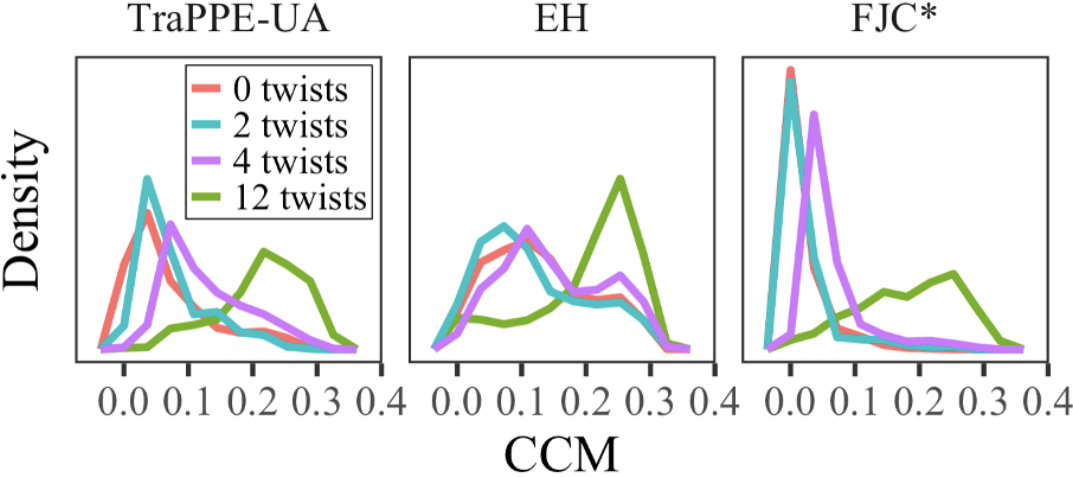


FIG. S3. Frequency polygons of normal modes binned by CCM for two-stranded polyethylene wires of length $N = 98$ at various levels of twist. Results are shown for (red) untwisted wire, (blue) 2 twists, (purple) 4 twists, and (green) 12 twists. Results are compared for (left) the TraPPE-UA model used in the main text, (center) an Explicit Hydrogen model, and (right) a variation of the Freely Joint Chain model (see Sec. I for details).

In addition to checking various lengths, we checked whether the trend persists across various force fields models. This is the

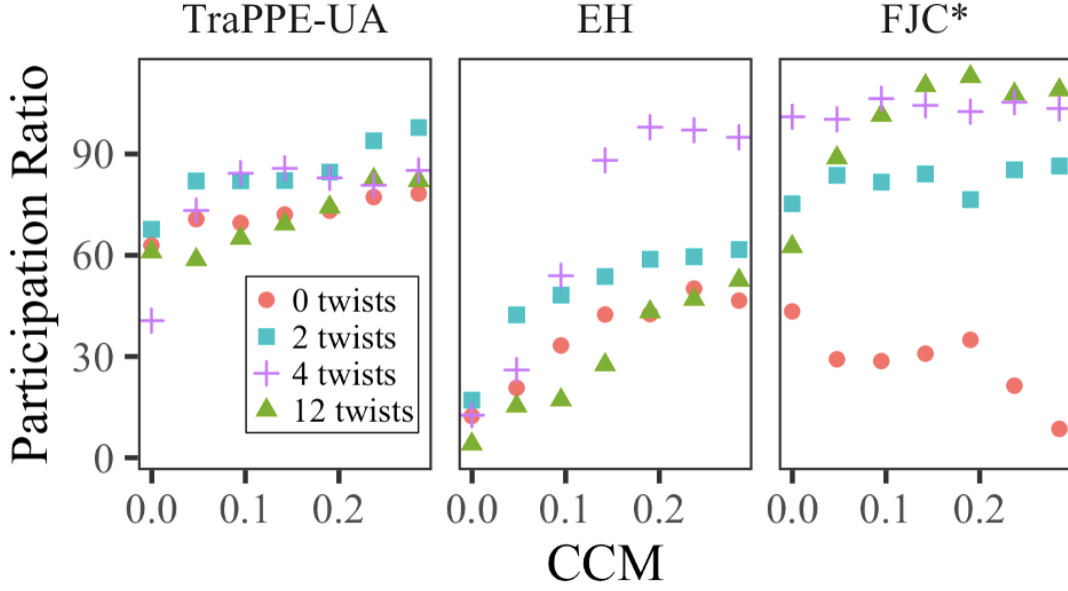


FIG. S4. Participation ratio coarse-grained by CCM bin for Frequency polygons of the normal mode distributions binned by CCM for two-stranded polyethelene wires of length $N = 98$ at various levels of twist. Results are shown for (red circles) untwisted wire, (blue squares) 2 twists, (purple crosses) 4 twists, and (green triangles) 12 twists. Results are compared for (left) the TraPPE-UA model used in the main text, (center) an Explicit Hydrogen model, and (right) a variation of the Freely Joint Chain model.

subject of Fig. S3 which compares (left) the results of the main text to analogous results using the other examined force fields (see Sec. I). The center panel shows an Explicit Hydrogen model which does not make the United Atom simplification. We see that the same trend, the shifting of the CCM distribution with twist, persists with this model as well. The right panel shows that the trend also persists using the FJC* model, which is the most reductionistic of the three examined.

We have also found a correlation between CCM and mode localization. A canonical localization measure for normal modes is the *participation ratio* (P_k) of mode k , varying from 1 when the vibrations are localized on a single atom to N if the mode is equally distributed on all atoms. The participation ratio is computed as follows: let the coefficients $u_{k,i}^\alpha$ denote the expansion of normal mode k in the atomic coordinates where α denotes the Cartesian coordinate and i denotes the atom number. Defining $p_{k,i} = \sum_\alpha |u_{k,i,\alpha}|^2$, the participation ratio is then defined as

$$P_k = 1 / \sum_i^N p_{k,i}^2. \quad (4)$$

Note that since we have taken the modes to be normalized, i.e. $\sum_i \sum_\alpha |u_{k,i,\alpha}|^2 = \sum_i^N p_{k,i} = 1$ [[S5, S7]].

Figure S3 shows that across a variety of force fields, the participation ratio is strongly correlated with the CCM in $N = 98$. This trend is persistent across various levels of twist, except for the untwisted wire in the FJC* model (note that the FJC* model is the least detailed and thus least physically accurate of the three force fields examined). This result suggests that the chiral modes could be involved in global transport properties of the molecule.

III. AXIAL CHIRALITY SPECTRA

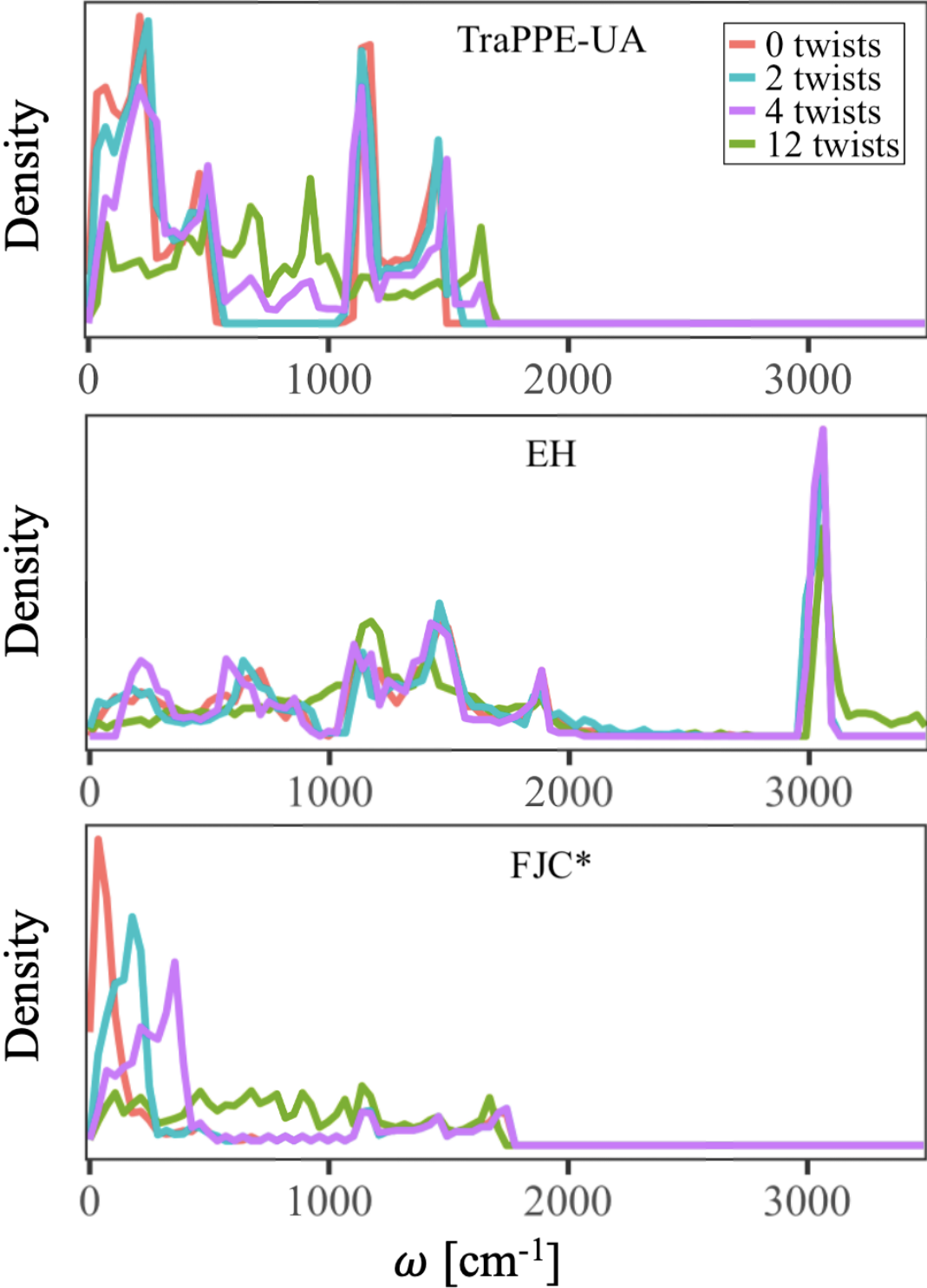


FIG. S5. Spectral densities binned by frequency for two-stranded polyethylene wires of length $N = 98$ at various levels of twist. Results are shown for (red) untwisted wire, (blue) 2 twists, (purple) 4 twists, and (green) 12 twists. Results are compared for (top) the TraPPE-UA model used in the main text, (middle) an Explicit Hydrogen model, and (bottom) a variation of the Freely Joint Chain model (see Sec. I for details).

In this section we demonstrate the persistence across various chain lengths and force fields of the second key finding of our main text, that momentum pseudoscalar score distribution is shifted in different directions for different frequency bands. Figure

S5 shows the spectral densities as a function of frequency for various levels of twist using three different force fields. The top panel shows data from the main text. Note the band gap (roughly between $\omega = 6 \text{ cm}^{-1}$ and $\omega = 1100 \text{ cm}^{-1}$) for 0 twists and 2 twists (red and blue line respectively). This band gap begins to disappear for 4 twists (purple line) and fully disappears for 12 twists (green line). For both other force fields, a similar band gap that fades with increased twist is present albeit less obvious. For the Explicit Hydrogen model (middle) this band gap is much narrower (appears at roughly $\omega = 1000 \text{ cm}^{-1}$), and for the FJC* model (bottom), the density of the high frequency band is greatly diminished. Note that in a structure with n particles and fixed center of mass, there are $3N$ normal modes (as mentioned in the main text, a small fraction returned imaginary frequencies; we discarded these from our analysis). Since there are $n = 588$ atoms in an $N = 98$ polyethylene double helix, this implies that there are 1764 total modes for the Explicit Hydrogen model. For the other force field models, which makes the United Atom simplification, there are only $n = 196$ total atoms and thus 588 normal modes. Because these details distract from our main point which is the shape of the distributions, we here and throughout the entire work we label our vertical axis with *density* (arb. u.). Note also that in only the EH model, there is a spike in the spectral density at roughly $\omega = 3000 \text{ cm}^{-1}$. We attribute this to modes involving motions of hydrogen atoms with minimal participation from the carbon atoms.

Figure S6 Shows the normal mode densities with respect to the axial chirality score (Eq. (5) in main text) for two two frequency ranges. The left panels were also shown in the main text. Remarkably, in all three models, when the wire is twisted, the axial chirality peak of the low frequency bands shifts to the right and that of the high frequency band shifts to the left. Note that although the peaks for the more detailed EH model (center) are less clearly defined, the general trend persists. The one exception is that in the EH model it appears that for the highly twisted structure (12 twists), the low frequency distribution shifts back towards zero. Lastly, note that for the highest frequency band in the Explicit Hydrogen model ($\omega \sim 3000 \text{ cm}^{-1}$), the corresponding peaks shifts to the right (result not shown). In total, these results suggest that structural chirality gives handedness to bands of the material's frequency spectrum. This is the result which has lead us to introduce the concept of *thermal chirality*.

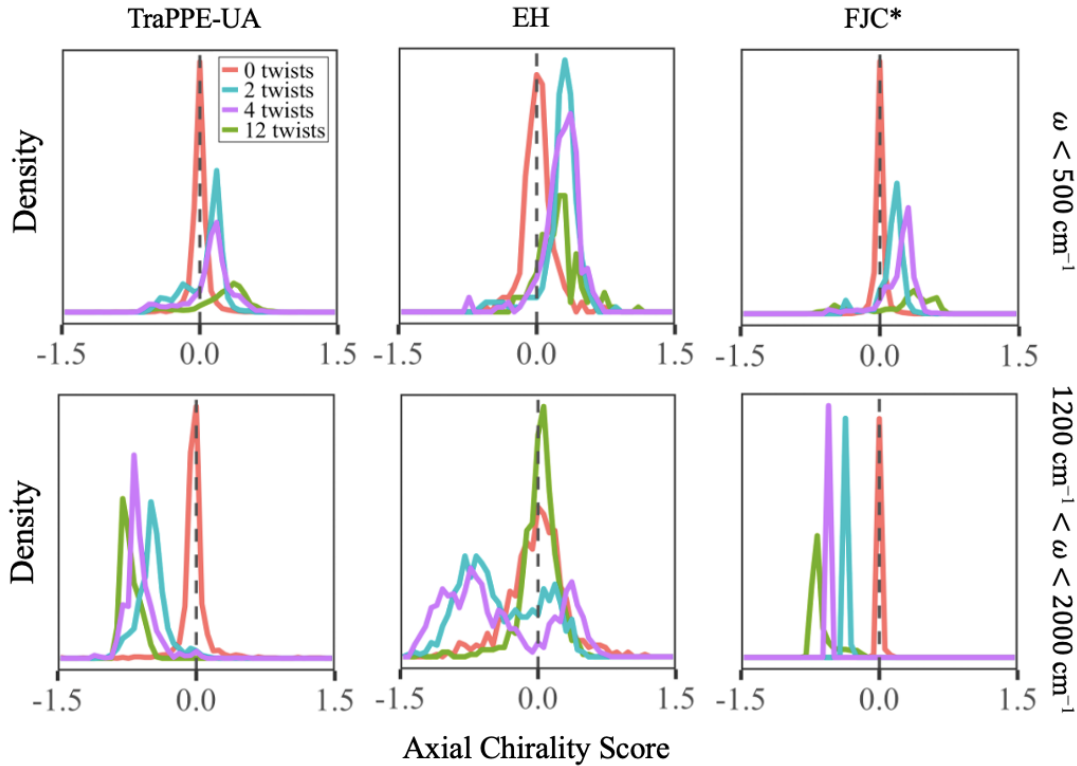


FIG. S6. Frequency polygons of normal modes binned by axial chirality score for $N = 98$ polyethylene double helical wires over particular frequency ranges. The (top) low frequency range is $\omega < 500 \text{ cm}^{-1}$ and the (bottom) high frequency range is $1200 \text{ cm}^{-1} < \omega < 2000 \text{ cm}^{-1}$. Results are shown for (red) untwisted wire, (blue) 2 twists, (purple) 4 twists, and (green) 12 twists. Results are compared for (left) the TraPPE-UA model used in the main text, (center) an Explicit Hydrogen model, and (right) a variation of the Freely Joint Chain model.

Figure S7 shows the mean and standard deviations of the distributions in these trends persist across various chain, and that the trends shown in Figure S6 persist across different chain lengths. Figure S7 also shows that although individual frequency bands are shifted by twist (center and right), the mean of the full spectrum remains near zero (left). It is therefore often necessary to observe individual frequency bands in order to find the chiral characteristics of normal mode spectra.

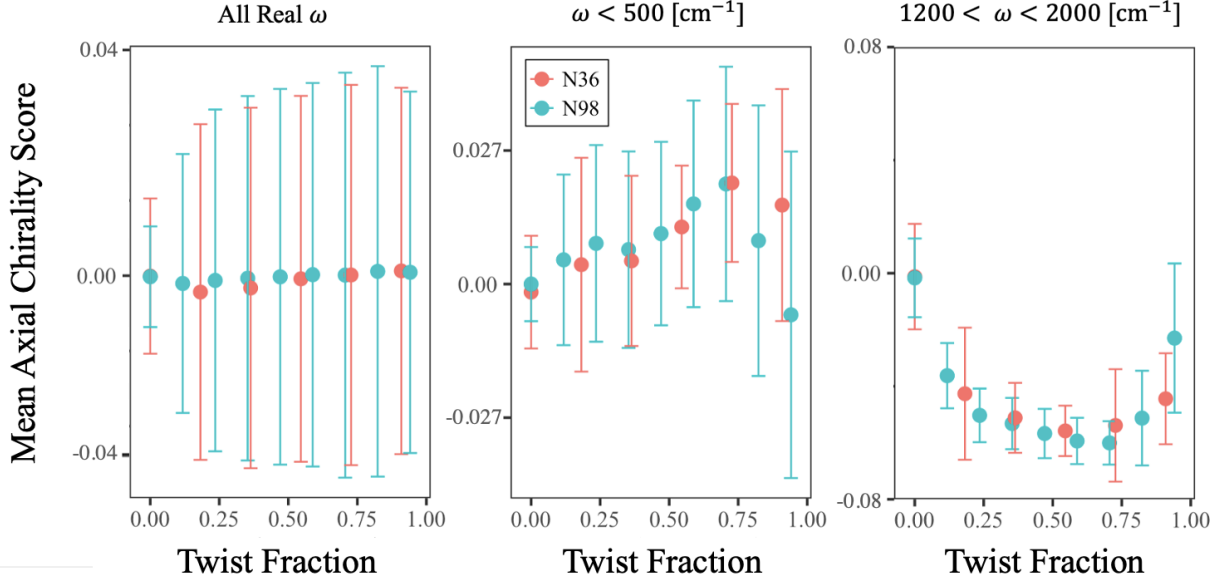


FIG. S7. The mean of the normal mode axial distributions for the TraPPE-UA force field as a function of the Twist Fraction given by $N_T/N_T^{\max}(N)$. Results are shown for lengths (red) $N = 36$ and (blue) $N = 98$, and over specific frequency ranges: (left) full spectrum, (center) $\omega < 500$ cm $^{-1}$, and (right) 1200 cm $^{-1} < \omega < 2000$ cm $^{-1}$. Error bars show the standard deviation of the distributions.

IV. SELECTION OF NORMALIZATION COEFFICIENTS

The main purpose of the scores used in this work is to assess the effect of twist on the shape of the distributions, and thus the exact magnitudes the scores take is of secondary importance. Nevertheless, we have given thought to choosing the best normalization coefficients so that the scores are dimensionless parameters taking on expected values $\ll 1$ for an arbitrary mode, and values ~ 1 for maximal scores. For the angular momentum scores (Eq. (4)) and axial chirality scores (Eq. (5)), the normalization coefficients are chosen so that unity is the maximum possible score for a mode that is perfectly delocalized (evenly distributed among all atoms) assuming a perfect helix with radius 1.5 Å. Note that with this approach, there are certain sequences of mode coefficients that could lead to scores higher than unity. Furthermore, as shown in Fig. S8, the helical radius (half the inter-chain distance) varies with the twistedness of the structure. However, despite these caveats, this method of normalization captures our desired qualitative behavior without introducing unnecessary mathematical convolution.

Specifically, for the case of $N = 196$ and $m_i = m$ for all i , the normalization constraint $\sum_i \Sigma_\alpha (u_{k,i}^\alpha)^2 = 1$ combined with perfect delocalization implies that $\sqrt{\langle u_{k,i} \rangle} = 1/\sqrt{196}$. Inspecting (Eq. (4)), the desired conditions occur when $|u_{k,i}\rangle = (u_{k,i}^x, u_{k,i}^y, 0)^T$ is perpendicular to $|r_i\rangle = (1/\sqrt{m_i})|q_i\rangle$ (with $\sqrt{\langle r_i \rangle} = 1.5$ Å) for all i . This all implies that

$$1 = A_1 \left| \sum_{i=1}^{196} m(1.5 \text{ \AA})(1/\sqrt{196}) \right| \quad (\text{S1a})$$

from which we obtain

$$A_1 = (21m \cdot \text{\AA})^{-1}. \quad (\text{S1b})$$

Similarly, inspection of (Eq. (5)) reveals that the desired conditions occur when both $|u_{k,i}\rangle = (u_{k,i}^x, u_{k,i}^y, 0)^T$ is perpendicular to $|r_i\rangle$ and $u_{k,i}^z = \sqrt{(u_{k,i}^x)^2 + (u_{k,i}^y)^2}$. This now implies

$$1 = A_2 \sum_{i=1}^{196} m(1.5 \text{ \AA})(1/\sqrt{2 \cdot 196})^2 \quad (\text{S2a})$$

from which we obtain

$$A_2 = (0.75m \cdot \text{\AA})^{-1}. \quad (\text{S2b})$$

Note that when we compare results for the EH and FJC* model (see Fig. S6), we use the same normalization coefficient as calculated for the TraPPE-UA model for simplicity.

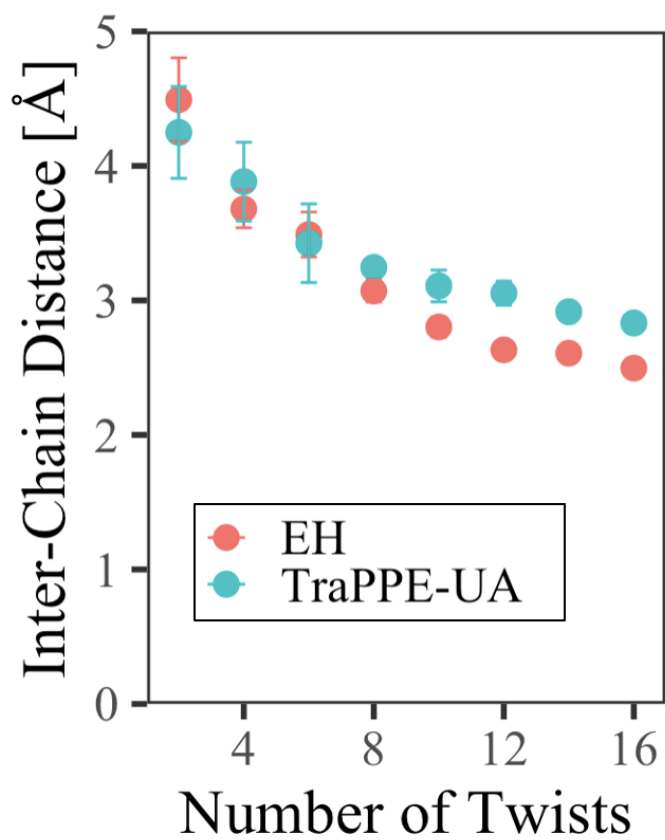


FIG. S8. Inter-chain distance between the chains in the double-helical polyethylene wire as a function of twist. Inter-chain distance is obtained by averaging several distances between corresponding atoms on opposite chains. Results are shown for (red) the Explicit Hydrogen model and (blue) the TraPPE-UA model. Standard deviations are shown when larger than symbol size.

REFERENCES: SUPPLEMENTAL INFORMATION

- [S1] M. Dinpajoo and A. Nitzan, *J. Chem. Phys.* **153** (2020), 10.1063/5.0023085.
- [S2] B. Chen and J. I. Siepmann, *J. Phys. Chem. B* **103**, 5370 (1999).
- [S3] S. J. Keasler, S. M. Charan, C. D. Wick, I. G. Economou, and J. I. Siepmann, *J. Phys. Chem. B* **116**, 11234 (2012).
- [S4] I. Sharony, R. Chen, and A. Nitzan, *J. Chem. Phys.* **153** (2020).
- [S5] E. Abraham, M. Dinpajoo, C. Climent, and A. Nitzan, *J. Chem. Phys.* (2023), 10.1063/5.0171680.
- [S6] M. Rubinstein and P. R. H. Colby, *Polymer Physics* (Oxford University Press, 2003).
- [S7] P. B. Allen and J. Kelner, *Am. J. Phys.* **66**, 497 (1998).